Filter method without boundary-value condition for simultaneous calculation of eigenfunction and eigenvalue of a stationary Schrödinger equation on a grid

M. Nurhuda[*] and A. Rouf

Physics Department, Faculty of Mathematics and Natural Sciences, Brawijaya University, Malang 65145, Indonesia

The paper presents a method for simultaneous computation of eigenfunction and eigenvalue of the stationary Schrödinger equation on a grid, without imposing boundary-value condition. The method is based on the filter operator, which selects the eigenfunction from wave packet at the rate comparable to δ function. The efficacy and reliability of the method are demonstrated by comparing the simulation results with analytical or numerical solutions obtained by using other methods for various boundary-value conditions. It is found that the method is robust, accurate, and reliable. Further prospect of filter method for simulation of the Schrödinger equation in higher-dimensional space will also be highlighted.

I. INTRODUCTION

Computations of eigenfunctions and eigenvalues of the stationary Schrödinger equation have been of great interest since the birth of quantum mechanics [1]. Solutions of the Schrödinger equation have many important applications in atomic and molecular physics, high energy physics, nuclear physics, and solid state physics; see, e.g., Refs. [2–5]. In general, the eigenfunction and eigenvalue problems of the stationary Schrödinger equation can be written in the form

$$H\phi_n = E_n\phi_n, \tag{1}$$

where H is the stationary Hamiltonian and E_n and ϕ_n are eigenvalue and eigenfunction, respectively. Having the solutions of the eigenvalues and eigenfunctions, one can further explore the properties of the physical system in which we are mainly interested. Also, it is possible to predict physical and chemical properties by purely *ab initio* calculations [6,7]. This explains the importance of the Schrödinger equation and its various applications in physics and chemistry.

Though the Schrödinger equation depicted in Eq. (1) seems simple, the actual computations of real physical or chemical problems are enormous challenges. Even modern computers often have trouble handling the excessive storage and computing times that are required. The reasons for these difficulties are manifold; apart from very few exceptions, such as the hydrogen atom, it is in general not possible to obtain the analytic solutions. For more complicated systems, one is forced to rely on a couple of compromises and approximations in order to keep the problem solvable. This leads into a simplified model of the Schrödinger equation such that it can be solved numerically.

To the best of our knowledge, the methods that are usually used to solve the stationary Schrödinger equation might be categorized into four, i.e., (i) the direct integration of stationary Schrödinger equation on grid, (ii) the diagonalization method, (iii) the relaxation method, and (iv) the spectral method.

The direct integration of the stationary Schrödinger equation utilizes the solutions at the boundary as a starting point (see, e.g., Refs. [8,9]). To obtain the solutions at the intermediate position, one has to propagate the solution at the boundary outward or inward. If there are two boundary conditions that have to be satisfied, the propagated solutions from the inward or outward direction must be matched in order to satisfy the continuity condition. Typically, an eigenvalue is estimated initially, and the converged eigenenergy and eigenfunction are obtained after a certain number of iteration, depending on the "stiffness" level of the problem of interest.

Methods in the second category rely on diagonalization of the Hamiltonian matrix which produces a complete set of desired eigenvalues (see, e.g., Refs. [10,11]). Limitations may exist if the eigenfunctions are expected to have very specific behavior due to complexity of the potential. To represent such a function, the number of basis functions to be used must be enormously large, and hence the storage and CPU time will be very demanding. Having obtained the eigenvalues, the eigenfunctions can be easily reconstructed from all involved basis functions.

The third category is based on the relaxation of the wave packet (see, e.g., Refs. [12–14]). This is realized by propagating the wave packet in imaginary time. As an arbitrary wave packet can be written as $\psi(\mathbf{r},t) = \sum_n a_n\phi_n(\mathbf{r})e^{-iE_n t}$, replacing t with $-i\tau$ can lead into decay of all states, except the state with lowest negative energy. As a result, the bound states grow exponentially with the biggest rate being on that having the deepest energy level, i.e., the ground state. To obtain higher excited eigenfunctions, the orthogonalization procedure is invoked which filters out the lower eigenfunction and hence forces the system to relax to an excited state [13].

The fourth category is the spectral method that utilizes the spectral properties of time evolution of the Schrödinger equation (see, e.g., Ref. [15]). The method requires the propagation of an initial wave packet to very long time, and computation of the correlation function $\mathcal{P}_I(t) = \langle\psi(\mathbf{r},0)|\psi(\mathbf{r},t)\rangle$ in each time step. By Fourier transforming the correlation function, one can obtain all eigenvalues that can be determined from the positions of sharp local maxima of $|\mathcal{P}_I(E)|^2$. The positions of the peaks show the position of desired eigenvalues E_n.

In this paper, we propose the filter method for simultaneous computation of eigenfunction and eigenvalue of the stationary Schrödinger equation on a grid. The idea behind the method is that any function or wave packet within a defined space can be expressed as a superposition of all eigenfunctions

*mnurhuda@ub.ac.id

such that, by applying an appropriate operator, one can basically select the specific eigenfunction from the wave packet. To pickup the eigenfunction, we implement the filter operator, which is defined as $F = 1/(H - E_n)$. It is expected that only the selected eigenfunction with $E = E_n$ survives, while other eigenfunctions whose energies are not matched, $E \neq E_m$, decease. Since the operator F acts globally on the space, the solution of the eigenfunction is independent of the boundary-value condition and hence determined by the Hamiltonian and the eigenenergy only. The present method thus not only provides a robustness in solving the eigenfunction and eigenvalue problem, but also a way to tackle the boundary-value problems.

Note that the filter method developed here is different from the filter method usually employed in image or signal processing. In signal processing, for example, filters can be devices, methods, processes, or mathematical operations that remove some unwanted frequency or signal components, while passing and optionally also modifying the others, e.g., high-, low-, or band pass components (see, e.g., Refs. [16,17]). The filters thus do not exclusively act in the frequency domain. In our method, on the contrary, the filter acts globally in a defined domain but only selects one component.

Our paper is organized as follows. In Sec. II we briefly review the underlying theory that is used to develop the method. In Sec. III we discuss the computational procedures for the 1D problem in a more detailed manner. To demonstrate the reliability of the method, in Sec. IV we present and discuss the simulation results of a 1D harmonic oscillator, the radial Coulomb wave function, and a 1D soft Coulomb potential, which represent various boundary-value problems in physics. In the next section, we briefly outline the strategy to implement the filter method in solving the coupled Schrödinger equation that usually appears in the many body problem. Finally, in Sec. VI the conclusions of our work are highlighted.

II. THEORY

The Schrödinger equation in general can be written as (unless otherwise specified, Hartree atomic units $e = m = \hbar = 1$, $c = 137$ are used thoroughly)

$$i \frac{\partial}{\partial t} \phi_n(\mathbf{r}) = H \phi_n(\mathbf{r}) = E_n \phi_n(\mathbf{r}), \tag{2}$$

which provides the solution of $\phi_n(\mathbf{r},t) = \phi_n(\mathbf{r}) e^{-iE_n t}$. The index n refers to either discrete or continuum. The stationary Hamiltonian H is given by

$$H = \left(-\frac{1}{2} \nabla^2 + V(r) \right). \tag{3}$$

Now, any wave packet can be expanded in a set of the respective eigenfunctions of Hamiltonian H,

$$\psi(\mathbf{r}) = \sum_n a_n \phi_n(\mathbf{r})$$

$$= \sum_b a_b \phi_b(\mathbf{r}) + \int_0^\infty dE_c a_c \phi_c(\mathbf{r}). \tag{4}$$

Here the index b stands for bound states, while c stands for continuum states.

We introduce a filter operator F, which has an explicit form of

$$F = \frac{1}{H - E_n}. \tag{5}$$

Applying the operator F on the wave packet $\psi(\mathbf{r})$, one can immediately obtain

$$F\psi(\mathbf{r}) = \frac{1}{H - E_n} \sum_m a_m \phi_m(\mathbf{r})$$

$$= \sum_m a_m \phi_m(\mathbf{r}) \delta(E_m - E_n)$$

$$= \tilde{\phi}_n(\mathbf{r}). \tag{6}$$

Thus, among all wave packet components, only the eigenfunction where its eigenenergy is matched with E_n will survive, while other components decay. Here, $\tilde{\phi}_n(\mathbf{r})$ refers to a filtered wave packet whose probability is peaked at $\phi_n(\mathbf{r})$, but is not yet normalized. Since the survivals of eigenfunctions are related to the δ function, the decaying rate of unwanted eigenfunctions would be comparable to the side lobes of the δ function. Equation (6) thus provides a rapid and robust computation method of eigenfunction and eigenvalue.

Let's say E_n^0 is the initial guess of the eigenvalue that is assumed to be close to the correct eigenvalue E_n and $\phi_n^0(\mathbf{r}) = \psi(\mathbf{r})$ is an initial continuous function; the steps of searching the eigenfunction and eigenvalue then read

$$\tilde{\phi}_n^1(\mathbf{r}) = \frac{\psi(x)}{H - E_n^0},$$

$$\phi_n^1(\mathbf{r}) = \frac{\tilde{\phi}_n^1(\mathbf{r})}{\sqrt{\int d^3r |\tilde{\phi}_n^1(\mathbf{r})|^2}},$$

$$E_n^1 = \int d^3r \, \phi_n^1(\mathbf{r}) H \phi_n^1(\mathbf{r}),$$

$$\tilde{\phi}_n^2(\mathbf{r}) = \frac{\phi_n^1(\mathbf{r})}{H - E_n^1},$$

$$\phi_n^2(\mathbf{r}) = \cdots,$$

$$E_n^2 = \cdots. \tag{7}$$

The process continues until the converged eigenfunction and eigenvalue are obtained.

III. NUMERICAL IMPLEMENTATION TO 1D PROBLEM

In this section, we discuss the computation procedures for the 1D problem in more detail. For a single particle moving in 1D space, the stationary Hamiltonian of the system can be written as

$$H(x) = -\frac{1}{2} \frac{\partial^2}{\partial x^2} + V(x). \tag{8}$$

Following Eq. (7), the implementation of the filter operator to the wave packet $\psi(x)$ then reads

$$\left(H(x) - E_n^k \right) \tilde{\phi}_n^{k+1}(x) = \phi_n^k(x), \quad \phi_n^0(x) = \psi(x), \tag{9}$$

where the superscript k stands for the kth iteration step. The initial function $\psi(x)$ can be be chosen to have the form

$$\psi(x) = \begin{cases} \sin(x) + \cos(x), & \text{for } -\infty < x < \infty, \\ \text{const} \neq 0, & \text{for } 0 < x < \infty. \end{cases} \tag{10}$$

Approximating the second order differential equation on $\tilde{\phi}_n(x)$ with a three-points finite different scheme, Eq. (9) leads into a tridiagonal system of equations with unknown $\tilde{\phi}_n^{k+1}(x)$:

$$\begin{bmatrix} \beta_1 & \gamma_1 & & & 0 \\ \alpha_2 & \beta_2 & \gamma_2 & & \\ & \ddots & \ddots & \ddots & \\ & & \alpha_{M-1} & \beta_{M-1} & \gamma_{M-1} \\ 0 & & & \alpha_M & \beta_M \end{bmatrix} \begin{bmatrix} \tilde{\phi}_n^{k+1}(x_1) \\ \tilde{\phi}_n^{k+1}(x_2) \\ \vdots \\ \tilde{\phi}_n^{k+1}(x_{M-1}) \\ \tilde{\phi}_n^{k+1}(x_M) \end{bmatrix} = \begin{bmatrix} \phi_n^k(x_1) \\ \phi_n^k(x_2) \\ \vdots \\ \phi_n^k(x_{M-1}) \\ \phi_n^k(x_M) \end{bmatrix}, \tag{11}$$

where the matrix elements for each iteration step are given by

$$\alpha_i = \gamma_i = -\frac{1}{2}\frac{1}{\Delta x^2},$$

$$\beta_i = \frac{1}{\Delta x^2} + V(x_i) - E_n^k. \tag{12}$$

Equation (11) can be easily solved by using a tridiagonal matrix solver which can be found elsewhere, e.g., Ref. [10]. Following Eq. (7) the new function $\tilde{\phi}_n^{k+1}(x)$ has to be normalized before computing E_n^{k+1}. The values of E_n^{k+1} and $\phi_n^{k+1}(x)$ are then used as inputs for the next iteration step. The process should continue until a convergent result is obtained.

IV. RESULTS AND DISCUSSIONS

In this section, we present simulation results of three different cases, i.e., 1D harmonic oscillator, radial Coulomb wave function, and 1D soft Coulomb potential. The 1D harmonic oscillator might represent a case where the solutions are strongly bounded around the origin, while the radial Coulomb wave function stands for the case where the boundary condition at the origin is close and the other side is free. The last one represents the boundary condition problem where both edges are free.

A. Harmonic oscillator

The Hamiltonian of a 1D harmonic oscillator is given by

$$H = -\frac{1}{2}\frac{\partial^2}{\partial x^2} + \frac{1}{2}Kx^2,$$

which provides the solution for energy $E_n = (n + \frac{1}{2})\omega$, with $\omega = \sqrt{K}$.

As $V(x) = \frac{1}{2}Kx^2$ becomes infinite at $x = \pm\infty$, the eigenfunction is strongly confined around the origin. The analytic solution of the eigenfunction has the form

$$\phi_n(x) = \left(\frac{\kappa}{\sqrt{\pi}n!2^n}\right)^{1/2} H_n(\kappa x)e^{-1/2(\kappa^2 x^2)},$$

with $\kappa = \sqrt{\omega} = K^{1/4}$ and $H_n(x)$ is the Hermite polynomial. The 1D harmonic oscillator thus represents a problem where the solutions are strongly bounded at both side edges.

For simulations, $K = \kappa^4 = 1$ was chosen. The x coordinate was spanned from -50 a.u to 50 a.u., and discretized into

$\Delta x = 0.01$ a.u. Following Eq. (10), an initial function $\psi(x) = \sin(x) + \cos(x)$ was chosen. This choice was taken in order to accommodate all eigenfunctions having odd and even parity.

Figure 1 (left) shows the simulation results for $n = 1, 50$, and 100, whereas the right panel displays the corresponding analytical results. It can be seen that the numerical eigenfunctions agree very well with the analytical ones. This indicates that the filter method is working well, even for cases where $n \gg 1$ and the respective eigenfunctions exhibit very fast oscillation.

The accuracy of the computed eigenenergies depends on the parameters of the spatial grid and n. Eigenfunctions with fast oscillation require finer grid and longer spatial range. Denoting $\epsilon = |\Delta E|/E$ as the relative error of the calculated eigenenergy with respect to the correct one, we found for $n = 100$, $\epsilon \approx 10^{-7}$, while for $n = 1$, we got $\epsilon = |\Delta E|/E \approx 10^{-10}$.

B. Radial Coulomb wave function

The stationary Schrödinger equation for atomic hydrogen can be written in spherical coordinate as

$$\left\{-\frac{1}{2}\left[\frac{1}{r^2}\frac{\partial}{\partial r}r^2\frac{\partial}{\partial r} + \frac{1}{r^2}\left(\frac{1}{\sin\theta}\frac{\partial}{\partial\theta}\sin\theta\frac{\partial}{\partial\theta}\sin\theta\right.\right.$$
$$\left.\left. + \frac{1}{\sin^2\theta}\frac{\partial^2}{\partial\vartheta^2}\right)\right] - \frac{1}{r}\right\}\psi(\mathbf{r}) = E\psi(\mathbf{r}). \tag{13}$$

By expanding $\psi(\mathbf{r})$ in a spherical harmonic basis function

$$\psi(\mathbf{r}) = \sum_{lm} G_{E,l}(r)Y_{lm}(\theta,\vartheta),$$

one can immediately obtain a set of decoupled radial Schrödinger equations which is 1D with r running from 0 to ∞,

$$\left(-\frac{1}{2}\frac{1}{r^2}\frac{\partial}{\partial r}\left(r^2\frac{\partial}{\partial r}\right) + \frac{1}{2}\frac{l(l+1)}{r^2} - \frac{1}{r}\right)G_{E,l}(r) = EG_{E,l}(r), \tag{14}$$

with l being the orbital quantum number. By substituting $G(r) = F(r)/r$, the radial part of Eq. (14) becomes

$$\left(-\frac{1}{2}\frac{\partial^2}{\partial r^2} + \frac{1}{2}\frac{l(l+1)}{r^2} - \frac{1}{r}\right)R_{E,l}(r) = ER_{E,l}(r). \tag{15}$$

As the potential is singular at $r = 0$, $R(r)$ must be bounded at the origin. The radial Coulomb wave function thus represents

FIG. 1. Comparison of computed eigenfunctions (left panel) with the corresponding analytical results (right panel) of 1D harmonic oscillator for various energy levels.

the 1D problem where the boundary value is well defined at the origin while at the other side edge is free.

The $G(r)$ and $R(r)$ normalize according to

$$\int_0^\infty G(r)G(r)r^2 dr = \int_0^\infty R(r)R(r)dr,$$

$$= \begin{cases} \delta_{nn'} & \text{for bound states,} \\ \delta(E - E') & \text{for continuum states.} \end{cases} \tag{16}$$

In the following, the numerical results of eigenenergies E and eigenfunctions $\phi_E(r)$ for $|E| \to 0$ are compared, both for discrete and continuum states. The calculation of eigenfunction for small E is of particular interest, since, to our experience, either the power series expansion or recurrence relation method [18] often fail when radial distance r becomes very large.

1. Bound states

The bound state solution for radial Coulomb wave function is given by [19]

$$R_{nl}(r) = N_{nl} e^{(-r/n)} \left(\frac{2}{n}r\right)^{l+1} F\left(-n+l+1, 2l+1, \frac{2r}{n}\right), \tag{17}$$

with N_{nl} being the normalization constant,

$$N_{nl} = \frac{1}{n} \frac{1}{(2l+1)!} \left[\frac{(n-l-1)!}{(n+l)!}\right]^{1/2},$$

and $F(a,b,x)$ being the confluent hypergeometric function.

For the sake of comparison, the principle quantum number $n = 25$ was chosen, providing $E = -0.0008$ a.u. Two angular momentum numbers were used, namely $l = 0$ and $l = 24$. The radial coordinate is stretched from $r = 0$ to $r_{\max} = 1800$ a.u. and discretized into $\Delta r = 0.1$ a.u. The results are shown in Fig. 2. Following Eq. (10), the initial wave function $\psi(r) = 1$ was chosen for all r.

It can be seen that the results obtained by using the filter operator (left panels) are identical to those analytical solutions (right panel). This is an indication that the method is working well even for simulating eigenfunction with extreme small energy. The accuracy of the computed eigenenergies with respect to the theoretical ones for high n is also excellent. With spatial parameters described above, for $l = 0$ we found $E_{25} = -7.9999627 \times 10^{-4}$ a.u., yielding the relative error $|\Delta E|/E \approx 10^{-6}$. For $n = 25$, $l = 24$ the calculated eigenenergy is even closer to the theoretical value, due to less oscillation of $R_{El}(r)$.

It is worth noting that, in performing the simulation, r must be set large enough in order to ensure that the wave function vanishes asymptotically. It is therefore important to make an
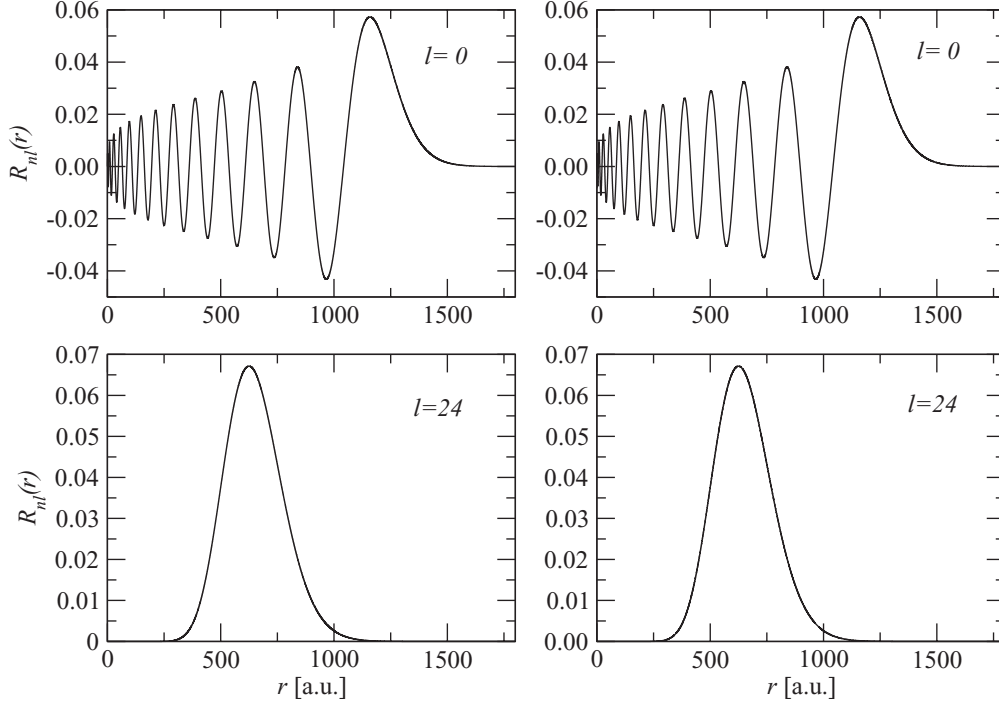
FIG. 2. Comparison of simulated bound state Coulomb wave functions of $n = 25$ and $l = 0$ (upper panel) and $n = 25$ and $l = 24$ (lower panel). Results in the left panels are obtained by using the filter method, while those at the right panels are computed using analytical formulas Eq. (17).

estimation for r_{max} prior to the simulation. We have learned that a rough estimation

$$r_{max} \approx \alpha 2.5 n^2 + \beta 10 n \qquad (18)$$

may be used. This relation is obtained by fitting r_{max} as a function of n. Here, $\alpha = \beta = 1$ are just constants in order that the left- and right-hand sides of Eq. (18) are of the same dimension. A better estimation might be derived by analyzing the asymptotic behavior of the Laguerre polynomial; see, e.g., Ref. [20].

2. Continuum states

The proposed filter operator is not only capable of simulating the bound state wave functions, but also works well for computation of continuum wave functions ($E > 0$). Unlike the bound states which are normalized to unity, the continuum states are normalized to a δ function. This requirement can lead into difficulty when simulating the continuum wave functions. It is therefore worth tackling the normalization problem that appears in the simulation of the continuum eigenfunction.

To overcome the problem, it is important to analyze the asymptotic behavior of radial differential equation (15). At $r \to \infty$ the terms which are proportional to $1/r$ and $1/r^2$ can be omitted. Consequently, the solution of R_{EL} at larger r must be of a sin- or cos-like function with amplitude equal to unity, which is in accordance with the analytical work (see, e.g., Ref. [21]). We adopted these properties to normalize the amplitude of $R_{El}(r)$ at large distance to unity.

For the sake of comparison, we chose the value of $E = 0.0005$ a.u., which is small enough to represent a case of $E \to 0$. Two angular quantum numbers were chosen, namely

$l = 0$ and $l = 20$. The radial distance was discretized into $\Delta r = 0.1$ a.u, with r_{max} set to 10 000 a.u. As an initial function we took $\psi(r) = 1$ for all r. The results are shown in Fig. 3; left panel stands for $l = 0$ and the right panel for $l = 20$. In both panels, the magenta (online color) curves represent results from simulations, while the red black curves from analytical ones. The analytic solutions were calculated using the Gautchi algorithm [18]. For a better view, we plotted only the results up to $r_{max} = 180$ a.u. for $l = 0$ and $r_{max} = 600$ a.u. for $l = 20$.

We can see that the results basically agree well with each other. A small discrepancy appears in the amplitude of the wave function, where in general the simulation results show slightly larger amplitude than that of analytical ones. We found that the discrepancies were originated from r_{max}, which was not large enough. By varying r_{max} to larger values, we found that converged results could be obtained after $r_{max} > 38\,000$ a.u.

On the contrary, the simulations of the wave function with larger E are relatively light and need a smaller value of r_{max}. For example, for $E = 0.5$ a.u. and $l = 20$, the value of $r_{max} = 400$ a.u. is large enough to provide convergent results.

Based on the numerical experiments, we found that the value of r_{max} might be estimated for arbitrary E as

$$r_{max} \approx \alpha \lambda^2 + \beta l^2,$$

where $\lambda = 2\pi/\sqrt{2E}$. Again, $\alpha = \beta = 1$ are just constants having the same meaning as Eq. (18). Thus, for large E, one just needs a small range of r_{max}, whereas for extremely small E, larger radial distance is necessary to guarantee the convergence of the calculated wave functions.
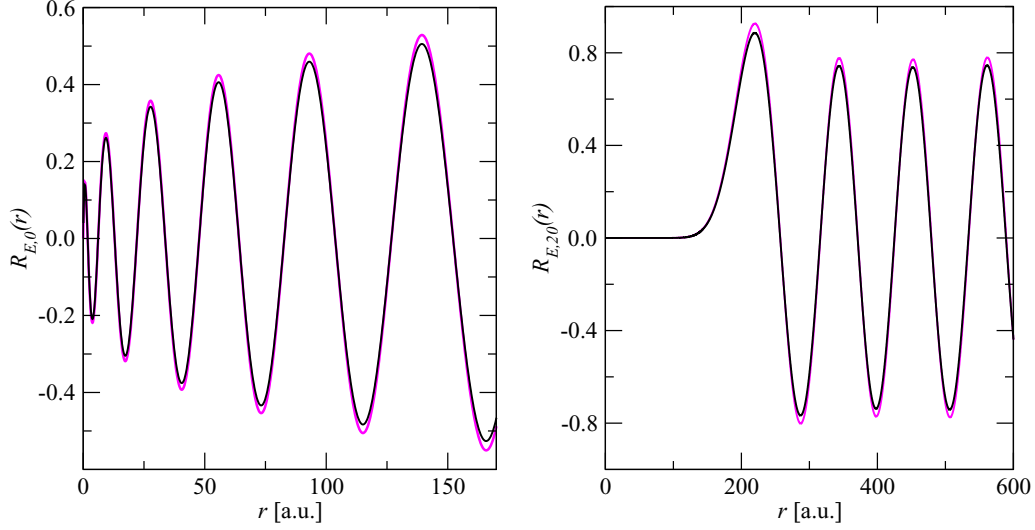
FIG. 3. Comparison of simulated eigenfunction of continuum Coulomb wave functions for $E = 0.0005$ a.u. and $l = 0$ (left panel) and $l = 20$ (right panel). The magenta (color online) curves stand for simulation results obtained by setting $r_{\max} = 10.000$ a.u., whereas the black curves are from analytic solutions.

C. Soft-Coulomb potential

The soft-Coulomb potential is a typical 1D problem where potential at both asymptotic edges vanishes. This potential has been used in a wide variety of applications requiring a 1D potential model, e.g., interaction of atom with intense laser field [22–24]. It has many attractive features including the removal of the singularity at zero while retaining a series of Rydberg states [25]. The 1D soft Coulomb potential is usually given in the form

$$V(a,x) = -\frac{V_0}{\sqrt{a + x^2}}, \quad -\infty < x < \infty, \tag{19}$$

where V_0 is the potential strength, chosen to be $V_0 = 1$, and a is the soft core parameter to remove the singularity at $x = 0$.

To the best of our knowledge, there is no existing analytical solution. It is therefore necessary to compare the results obtained by the present method with simulation results by using another method. We chose the relaxation method [12,13,26], since this method guarantees that the first result of the eigenenergy is the ground-state energy.

For that purpose, we performed a series of simulations with various parameter a. The spatial coordinate x was set from $x_{min} = -200$ a.u. to $x_{\max} = 200$ a.u. and discretized into $\Delta x = 0.01$ a.u. $\psi(x) = \sin(x) + \cos(x)$ was chosen for the initial wave function. The ground energy for each a was scanned by inputting the initial guess E_0 ranging from -4 a.u. to 0 a.u. with an increment of $\Delta E = 0.005$ a.u. The lowest negative energy was then considered as the ground-state energy.

The simulation was repeated for every new parameter a, until all ground-state energies for $a = 0 \to 2.5$ a.u. were obtained. The increment of Δa was chosen as 0.01 a.u. Note that, for $a = 0$, the potential transforms itself from the soft Coulomb to the hard core Coulomb potential. The avoid the singularity at $x = 0$, we added a very small positive number $\epsilon = 10^{-15}$, such that at $x = 0$, $V(a = 0, x = 0) = -1/\sqrt{\epsilon}$.

For the simulation using the relaxation method we employed Crank Nicholson to advance the solution from t to $t + \Delta t$ [10]. By replacing the real time t with $-i\tau$ we get

$$\psi(x, \tau + \Delta\tau) = \frac{1 - H\Delta\tau/2}{1 + H\Delta\tau/2}\psi(x, \tau). \tag{20}$$

Note that the scheme (20) is not unitary and hence the solution for $\psi(x, \tau)$ must be normalized after every time step. All spatial parameters were chosen to be the same with that used in the filter method, while the propagation time τ was evolved with $\Delta\tau = 0.05$ a.u., that is small enough to guarantee the correct solution. The maximum propagation times $\tau_{\max}$ were varying for each E_0. In this simulation, an initial function $\psi(x, \tau = 0) = 1$ was used for all x.

In Fig. 4, the simulation results of ground-state energy obtained by filter operator method (left panel) are displayed together with those obtained by using relaxation method (right panel). We can see that both curves agree very well with each other. The cusps also exist in both curves.

To analyze the origin of the cusp, in Fig. 5, we show the calculated ground-state eigenfunctions $\phi_0(x)$ for three different values of a, i.e., black curve for $a = 0$ a.u., red (color online) curve for $a = 0.01$ a.u., and orange (color online) curve for $a = 2$ a.u. We can see that, for $a = 0$ a.u., the wave component at the left side $\phi_0(x < 0)$ is totally decoupled from the wave component at the right side $\phi_0(x > 0)$. This is because the potential $V(0, x)$ which is singular at $x = 0$ behaves like an infinite wall such that it avoids the wave components from a different side axis to interact. Consequently, the wave component along the left axis is exactly the same as that at the right axis. As a increases, the potential $V(a, x)$ transforms from purely Coloumbic to a potential valley with a depth $-1/\sqrt{a}$ and of full width at half maximum (FWHM) equal to $2\sqrt{3}a$. As a result, the particle is confined around the origin (red curve). However, as a increases, the potential becomes more flattened and widened, such that the wave function becomes
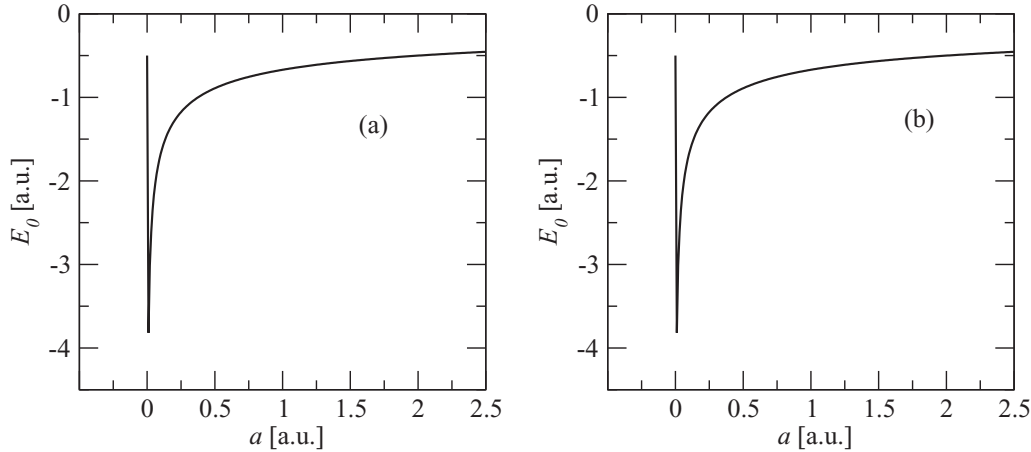
FIG. 4. Ground-state energy of soft Coulomb potential for various soft core parameters a obtained by using (a) filter method and (b) relaxation method.

less confined, as can be seen in the blue curve. This explains why the curve of the eigenenergy displays a cusp.

Rydberg energy levels of soft Coulomb potential

It is believed that the soft Coulomb potential provides rich Rydberg energy levels. A question may arise as to how different the Rydberg energy levels of the soft Coulomb potential are with respect to Rydberg energy levels in the hydrogen atom.

For that purpose, we performed a series of simulations for each parameter a with input energy varied from -4.0 a.u to 0 a.u., and with increment $\Delta E = 0.005$ a.u. The calculated eigenenergies were then sorted from the lowest value to the highest one. The simulations were repeated with another value of parameter a. The smallest a was 0.01 a.u. and increased to $a = 2.5$ a.u. with an increment $\Delta a = 0.01$ a.u. As an initial wave function, we chose $\psi(x) = \sin(x) + \cos(x)$.

In Fig. 6 we plot the series of eigenenergies of the first 10 excited states as a function of a. By carefully elaborating the wave functions, we found that eigenenergies labeled with odd numbers own odd parity eigenfunction (antisymmetry wave function), while those with even number are of eigenfunctions

with even parity. In particular, for $a = 2$ a.u, even the ground-state energy is exactly the same with the ground-state energy of the hydrogen atom, but the excited state energies are largely different. To be more specific, the values of $E_1 = -0.233$ a.u., $E_2 = -0.134$ a.u., $E_3 = -0.0845$ a.u. ..., are deeper than the corresponding excited energy of atomic hydrogen $E_1 = -0.125$ a.u., $E_2 = -0.055$ a.u., $E_3 = -0.03125$ a.u. ..., by about a factor more than 2.

The reason that the soft Coulomb potential yields higher excited energy can be tracked from the range of potential domain; in the case of $-\infty < x < \infty$, the potential forms a symmetric valley. The electron thus experiences wider effective potential than that in pure Coulomb potential ($0 < r < \infty$). In a separate simulation using soft Coulomb potential with $a = 2$, while the range of x is set from ($0 < x < \infty$), we found $E_0 = -0.234$ a.u, $E_1 = -0.085$ a.u., $E_2 = -0.0429$ a.u., etc., which are now much smaller than the corresponding energy level of the hydrogen atom.

V. APPLICATION OF FILTER METHOD FOR COUPLED PARTIAL SCHRÖDINGER EQUATION

To this end, we have discussed problems in purely 1D or in terms of decoupled radial Schrödinger equations. A question
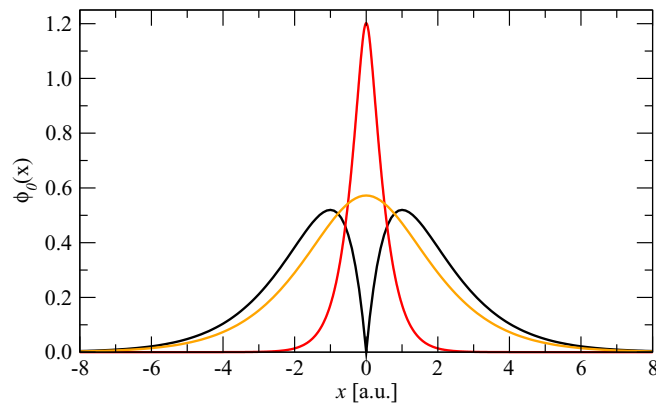
FIG. 5. Comparison of the simulated ground-state eigenfunctions of soft Coulomb potential for three different values of a, i.e., $a = 0$ a.u. displayed as black curve, $a = 0.01$ a.u. as red (online) curve, and $a = 2$ a.u. as orange (online) curve.
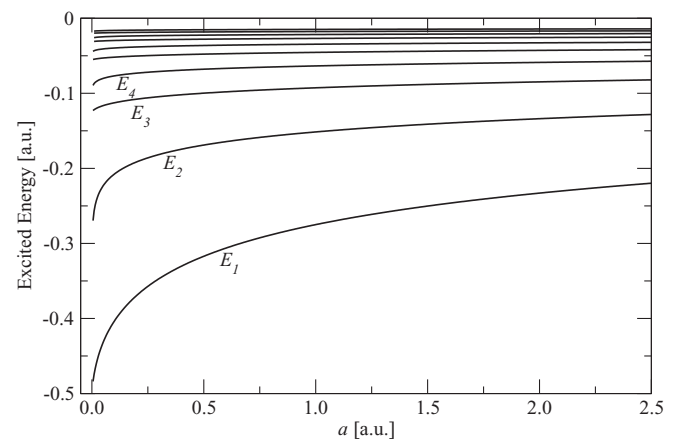
FIG. 6. Plot of the first 10 Rydberg energy levels of soft Coulomb potential as a function of soft core parameter a.

arises whether the method is applicable to the problem where the radial differential equations are coupled with each other. For example, in the two electron atom system, the wave function is a function of electron coordinates $\mathbf{r}_1$ and $\mathbf{r}_2$. If for every $\mathbf{r}_i$ there are a pair of $\{x_i, y_i, z_i\}$, then there are six independent variables.

The computational strategy to solve such problems can be briefly outlined as follows. First, the wave function is presented in the hyperspherical coordinate system (see, e.g., Refs. [27,28]),

$$\psi(\mathbf{r}_1, \mathbf{r}_2, \ldots) = \sum_\mu R_\mu(\rho) \mathcal{Y}_\mu(\alpha_1, \ldots, \Omega_1, \Omega_2, \ldots), \quad (21)$$

where ρ is the hyperradial coordinate and α is a pseudoangle coordinate that is used to decompose the hyperradial coordinate ρ into individual radial coordinates. The index μ is a collection of individual indices $\mu \equiv \{\nu, \ldots, l_1, l_2, \ldots, m_1, m_2 \ldots\}$, with ν is an index of polynomial degree when transforming $f(r_1, r_2 \ldots) \to \sum g_\nu(\rho) h_\nu(\alpha_1, \ldots)$. The hyperspherical harmonic functions must be chosen in order that they satisfy the orthonormal condition

$$\int_{\alpha,\ldots,\Omega\ldots} \mathcal{Y}_\mu^*(\alpha_1, \ldots, \Omega_1, \Omega_2, \ldots) \mathcal{Y}_{\mu'}(\alpha_1, \ldots, \Omega_1, \Omega_2, \ldots) d\alpha \ldots d\Omega_1 d\Omega_2 \ldots = \delta_{\mu\mu'}. \quad (22)$$

For a two electron atom system, ρ may be chosen as $\rho = \sqrt{r_1^2 + r_2^2}$ and $\alpha = \tan^{-1}(r_2/r_1)$. The two electron wave function can be written as

$$\psi(\mathbf{r_1}, \mathbf{r_2}) = \sum_{l_1 l_2 m_1 m_2} G_{l_1 l_2}(r_1, r_2) C_{m_1 m_2 0}^{l_1 l_2 L} y_{l_1 m_1}(\theta_1, \vartheta_1) y_{l_2 m_2}(\theta_2, \vartheta_2)$$

$$= \sum_{\nu l_1 l_2 m_1 m_2} G_{\nu l_1 l_2}(\rho) J_{l_1 l_2}^\nu(\alpha) C_{m_1 m_2 0}^{l_1 l_2 L} y_{l_1 m_1}(\theta_1, \vartheta_1) y_{l_2 m_2}(\theta_2, \vartheta_2)$$

$$= \sum_{\nu l_1 l_2 m_1 m_2} \frac{R_{\nu l_1 l_2}(\rho)}{\rho^{5/2} \sin\alpha \, \cos\alpha} J_{l_1 l_2}^\nu(\alpha) C_{m_1 m_2 0}^{l_1 l_2 L} y_{l_1 m_1}(\theta_1, \vartheta_1) y_{l_2 m_2}(\theta_2, \vartheta_2). \quad (23)$$

Here, $J_{l_1 l_2}^\nu(\alpha)$ is Jacobi polynomial and $C_{m_1 m_2 0}^{l_1 l_2 L}$ is the Clebsch-Gordon coefficient. Following Eq. (7), the iteration procedures to select the eigenfunction must satisfy

$$\left(H - E_n^k\right) \phi_n^{k+1}(\mathbf{r}_1, \mathbf{r}_2, \ldots) = \phi_n^k(\mathbf{r}_1, \mathbf{r}_2, \ldots). \quad (24)$$

Again, the superscript k is used to label the iteration number. Now, expanding both $\phi_n^{k+1}(\mathbf{r}_1, \mathbf{r}_2, \ldots)$ and $\phi_n^k(\mathbf{r}_1, \mathbf{r}_2, \ldots)$ according to Eq. (21), multiplying with $\mathcal{Y}_{\mu'}^*(\alpha_1, \ldots, \Omega_1, \Omega_2, \ldots)$, and then integrating over whole solid angles $d\alpha \ldots d\Omega_1 d\Omega_2 \ldots$, we get a set of coupled Schrödinger equations in hyperradial coordinates:

$$\left(H_{\mu\mu}(\rho) - E_n^k\right) R_\mu^{k+1}(\rho) + \sum_{\mu \neq \mu'} H_{\mu\mu'}(\rho) R_{\mu'}^{k+1}(\rho) = R_\mu^k(\rho).$$

$$(25)$$

This set of coupled hyperradial Schrödinger equations (25) can be solved using the matrix-iterative method, described elsewhere, e.g., in [29].

VI. CONCLUSIONS

In conclusion, we have developed a filter method for simultaneous computation of eigenfunction and eigenvalue of a stationary Schrödinger equation on a grid, without imposition of boundary conditions. The filter operator is chosen to have the form of $1/(H - E)$, such that when the filter operator is exerted on an arbitrary continuous wave function, the desired eigenfunction is singled out at the rate of the δ function.

The comparison of the results with the well known 1D solvable problems show an excellent agreement with each other, e.g., harmonic oscillation and Coulomb wave function, which indicates the reliability of the method. In the case of Coulomb potential, we also provided an approximation of maximum radial distance $r_{\max}$ to be set in simulations, both for discrete and continuum wave functions.

In further simulations, we studied the eigenenergy of ground and excited states of the Hamiltonian with soft Coulomb potential $V(a,x) = -1/\sqrt{a + x^2}$. We found that the curve of eigenenergy displays a cusp, which is apparently due to the transforming behavior of the potential from Coulombic to 1D potential valley. We further found that, for $a = 2$ a.u., the ground-state energy is the same as the ground state of the hydrogen atom, but the excited energies in general are deeper by a factor more than twice that of the corresponding excited energy levels in the hydrogen atom.

Finally, by presenting the wave function in a hyperspherical coordinate, one can expect to further implement the filter method to solve the stationary Schrödinger equation for a many electron system.

[1] See, e.g., A. Messiah, *Quantum Chemistry* (North-Holland, Amsterdam, 1967).

[2] F. H. M. Faisal, *Theory of Multiphoton Processes* (Plenum, New York, 1987).

[3] I. N. Levine, *Quantum-Chemistry* (Prentice-Hall International, Upper Saddle River, NJ, 2000).

[4] G. D. Mahan, *Many-Particle Physics*, 3rd ed. (Springer Science+Business Media, New York, 2000).

[5] I. V. Puzynin, T. L. Boyadzhiev, S. I. Vinitskii, E. V. Zemlyanaya, T. P. Puzynina, and O. Chuluunbaatar, Phys. Part. Nucl. **38**, 70 (2007).

[6] T. C. Chen, J. Chem. Phys. **23**, 2200 (1955).

[7] C. C. J. Roothaan, J. Chem. Phys. **28**, 982 (1958).

[8] T. E. Simos, Comput. Math. Appl. **33**, 67 (1997).

[9] V. Fack, H. De Meyer, and G. Vanden Berghe, J. Comput. Appl. Math. **20**, 211 (1987).

[10] W. H. Press, S. A. Teukolsky, W. T. Vetterling, and B. P. Flannery, *Numerical Recipes*, 2nd ed. (Cambridge University Press, Cambridge, UK, 1992).

[11] G. H. Golub and C. F. Van Loan, *Matrix Computation*, 3rd ed. (The Johns Hopkin University Press, Baltimore, 1996).

[12] J. W. Neuberger and D. W. Noid, Chem. Phys. Lett. **104**, 1 (1984).

[13] R. Kosloff and H. Tal-Ezer, Chem. Phys. Lett. **127**, 223 (1986).

[14] P. Bader, S. Blanes, and F. Casas, J. Chem. Phys. **139**, 124117 (2013).

[15] M. D Feit, J. A Fleck, Jr., and A. Steiger, J. Comput. Phys. **47**, 412 (1980).

[16] S. W. Smith, *Digital Signal Processing* (California Tech. Pub., San Diego, CA, 1999).

[17] P. Stoica and R. Moses, *Spectral Analysis of Signal* (Prentice-Hall, Englewood Cliffs, NJ, 2005).

[18] W. Gautschi, Commun. ACM **9**, 793 (1966).

[19] L. D. Landau and E. M. Lifshitz, *Quantum Mechanics Non-Relativistic Theory*, 3rd ed. (Pergamon Press, Oxford, 1991).

[20] N. M. Temme, J. Appl. Math. Phys. **41**, 114 (1990).

[21] M. Abramowitz and I. A. Stegun, in *Handbook of Mathematical Function*, Applied Mathematic Series Vol. 55 (National Bureau of Standards, Gaithersburg, MD, 1964), p. 542.

[22] U. Schwengelbeck and F. H. M. Faisal, Phys. Rev. A **50**, 632 (1994).

[23] M. Stroe, I. Simbotin, and M. Gavrila, Phys. Rev. A **78**, 033405 (2008).

[24] T. Dziubak and J. Matulewski, Eur. Phys. J. D **59**, 321 (2010).

[25] T. E. Baker, E. M. Stoudenmire, L. O. Wagner, K. Burke, and S. R. White, Phys. Rev. B **91**, 235141 (2015).

[26] S. A. Chin, S. Janecek, and E. Krotscheck, Chem. Phys. Lett. **470**, 342 (2009).

[27] A. F. Starace, in *Fundamental Processes of Atomic Dynamics*, edited by J. S. Briggs, H. Kleinpoppen, and H. O. Lutz (Plenum, New York, 1988).

[28] X. Yang, J. Xi, C. G. Bao, and C. D Lin, Phys. Rev. A **52**, 2029 (1995).

[29] M. Nurhuda and F. H. M. Faisal, Phys. Rev. A **60**, 3125 (1999).